Proceedings of the 25th International Conference on
Port and Ocean Engineering under Arctic Conditions
June 9-13, 2019, Delft, The Netherlands

Marine spray from wave run-up to a hull as input to icing models

Albert B. Aalbers[1] and Jeroen S. Hoving[2]
[1] Retired from Maritime Research Institute Netherlands, Renkum, the Netherlands
[2] Delft University of Technology, Delft, the Netherlands

ABSTRACT

Ships at sea will encounter deck wetness events that usually are just annoying and rarely lead to damage. Discomfort is experienced by spray, as it is limiting view and hampering deck work. In freezing conditions, deck wetting will lead to icing.

This study is a continuation of publications regarding the development of a marine icing model based on spray predictions, taking into account ship shape and the physics of wave run-up leading to spray jets. The modelling of jet development from wave run-up against a wall, representing a ship hull, is investigated by experiments and mathematical modelling using nonlinear wave theory. Run-up jets occur frequently for ships at sea and are responsible for most of the generated spray. Detailed measurements of the run-up jet were obtained from high-speed video registration yielding information on the droplet distribution. The measurements indicate that the thickness of the run-up jet above the wall determines the maximum droplet size, and that this size is significantly larger than generally assumed in icing models. Based on these insights, new computations are performed with the 'SHIPICE' marine icing model to demonstrate the applicability and accuracy of the approach.

KEY WORDS: Wave run-up; Spray jets; Icing; Experiments; Computational Modelling;

NOMENCLATURE:

β	angle between wave front and wall	dt	time step in jet	k_o	overtopping ratio
ε	phase of wave, equal to ωt	dS	area element in wave crest	K	steepness enhancement factor
θ	wall angle	d	water depth	ΔE_k	nonlinear kinetic energy
Δh	wave crest enhancement due to ΔE_k	d_{mm}	mass mean drop diameter	m	mass per unit width of dS
$\delta_{root,\,i}$	jet root thickness for i^{th} element	c_o, c_{nl}	linear, nonlinear wave celerity	E_p	potential energy
λ_{tt}	trough-trough wave length	f	H_c/H_t	t	time for ballistic flight
μ	wave direction	f_1	single crest enhancement factor	T	observation time
μ_w	dynamic viscosity water	f_2	reflected crest enhancement factor	u_{lin}	horizontal orbital wave velocity
ρ	water density	g	standard gravity	$v_{jet,i}$	initial jet velocity of i^{th} element
σ_w	surface tension	H_c	crest height	X_{wr}	x-coordinate of reflected wave
ω	angular frequency	H_t	trough depth	$X_{F/A,i}$	fore, aft position of i^{th} jet element
A_{lin}	linear wave amplitude	$H_{\max,i}$	max. height of i^{th} jet element	Z_{wr}	z-coordinate of reflected wave
Cr_{elev}	crest elevation at wall	k, k'	wave numbers: $2\pi/\lambda_{tt}, 4\pi/\lambda_{tt}$	Z_i	vert. position of i^{th} jet element

1. INTRODUCTION

In the last decade, significant research work has been carried out, e.g. Buchner et al. (1998, 2004) and Ogawa et al. (2004), to develop methods to compute green water events from wave crests exceeding the bow, and to compute the corresponding flow over the deck as well as possible impacts on deck structures. Buchner (2001) and Fekken (2004) have presented volume of fluid methods that provide apparently realistic flow patterns even though its load predictions were less satisfactory. However, spray is generally considered of less importance then 'green water', or overtopping as it is referred to in hydraulic research (Hofland et al. (2015)).

Yet, in cold weather when spray water may lead to severe icing, deck wetting is of interest due to the relative frequency of occurrence of spray in a seaway. The development of spray and related deck wetting has recently been subject of investigation in marine research by Aalbers and Poen (2015) and Hoes et al (2016). Aalbers and Poen (2015) present a first attempt to quantify the amounts of spray water ejected at the bow of a ship in a seaway, taking into account bow flare and bow wave. In this research, it was shown that run-up of waves may lead to upward jetted spray. Even though a lot of the spray lands next to the ship, the spray volume is quite significant and may include large blobs of water. When these blobs do land on the ship, they cause a water flow over the deck that resembles 'green water' events, even though the resulting water volume on deck is smaller than the volumes for overtopping events.

1.1 Amounts of spray above bulwark

The amount of spray water exceeding the bulwark height may be quite significant, not in the least because of its high frequency of occurrence. Further aspects that play a role here are:

1. Spray is mostly caused by run-up against the flare of incoming wave and bow wave combined, and only incidentally by a wave slam.
2. It occurs in a 'choppy' sea state which is still relatively mild and in which the ship is not moving (pitching) a lot.
3. Run-up yields no impact, so that the shipmaster does not change course or slow down.

In 'choppy' conditions, the crest of the incoming wave frequently accelerates and develops a jet against the hull that may exceed the bulwark height. An example of the amounts predicted for a 120 m frigate type hull form in a sea state with 5 m significant wave height is given in Figure 1 that is taken from Aalbers and Poen (2015). The figure shows speed dependence and direction dependence. For run-up, apparently, changing course may not always help.

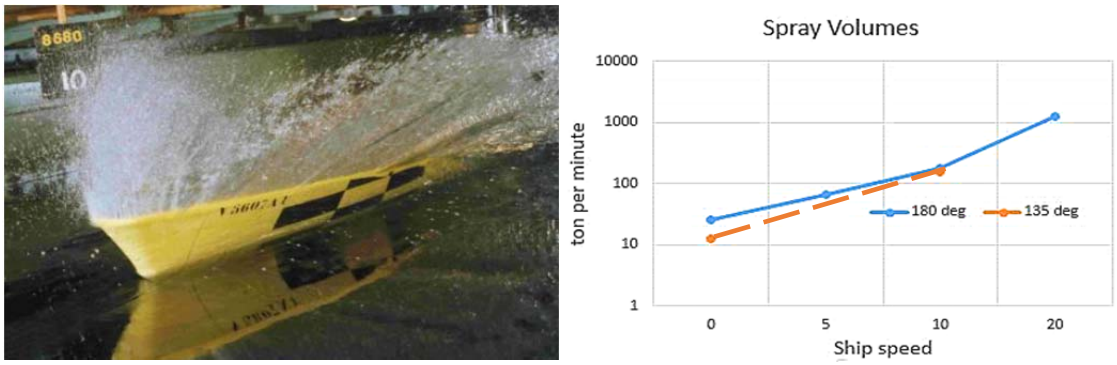

Figure 1: Effect of speed and wave direction in a H_s = 5 m sea state for a 120 m long frigate hull at 20 kn., after Aalbers and Poen, 2015.

1.2 Spray water model

Aalbers and Poen (2015) presented a computational method to determine the spray water that uses the physical particulars of ship shape and deals with an irregular sea state in a stochastic approach, where linear ship motion codes are used to compute the relative water velocities around the bow. Furthermore, the hydrodynamic model of wedge entry by Faltinsen (2002) was parameterized to obtain a fast analytic computation scheme for the jet root thickness and velocity. Aalbers and Poen include gravity for the jet elevation along the ship flare, but use Faltinsen's model for jet volume.

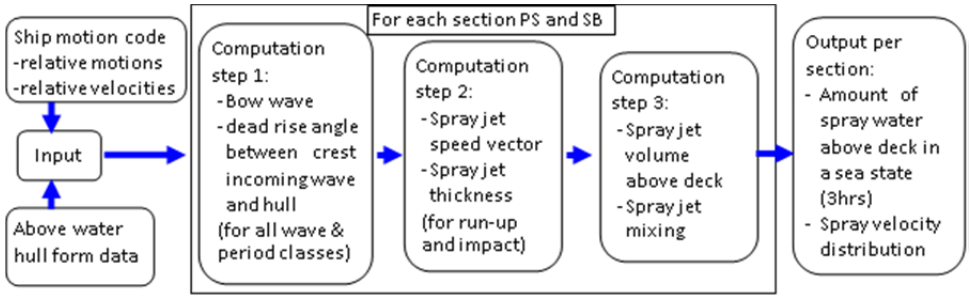

Figure 2: Computation scheme for spray water amounts above the bulwark (deck) of a ship in waves.

Additionally, they applied an analytical model of bow wave development from Noblesse et al. (2011) to incorporate its important additional vertical velocity component to the water movement along the bow flare. The analytical approach is chosen as such to compute the large statistical sum of wave heights and periods in a sea state for a range of locations around the bow in an acceptable computer effort. The computational scheme is shown in Figure 2.

1.3 Water on deck

The water in the spray jet above the bulwark will fall back due to gravity. Depending on the speed of the ship and the wind acting on it, part of it falls on deck. Generally, a ship has an outward flare angle so that, in a ship-fixed coordinate system, the water has an outward velocity component. The ensuing ballistic process has been described by Hoes et al (2016). Important for this process is the droplet size in the spray jet. Several authors investigating deck wetting, e.g. Kulyakhtin (2014) and Horjen (2015), have taken a characteristic value of the droplet size, assuming that impact-like phenomena cause the spray. Sub-millimeter droplet sizes were thus used in those calculation models. However, the run-up spray jet is up to several decimeters thick and the break-up process is not very strong, as explained in section 3.3 of this paper. Additionally, gravity causes some 'clustering' of water due to the slow-down of the vertical component of the spray jet speed. Henceforth, large drops - here defined as blobs - of water are formed. The amount of water in these relatively slowly moving blobs may be significant (order of m^3) and be the cause of a thin layer of water on deck.

1.4 Outline of the paper

The intent of this paper is to present the development of an improved method to quantify the water volume in spray events and thereby improve the ability to quantify the water volume wetting the ship surface. Previously, Aalbers and Poen (2015) used an engineering approach by applying an estimated correction factor (in the volume computation method) to obtain a realistic agreement of their results with the scarcely available experimental data.

The wave run-up experiments that were carried out at MARIN are described in Section 2. In Section 3, the wave run-up and jet formation model, that includes overtopping, is summarized and validated by comparison with the wave run-up tests. Section 4 shows that, despite proposed improvements to the method, a jet volume correction factor is still required, but can be computed. In section 5, the new results are used to compute icing for a heavy icing event and to demonstrate and discuss some important dependencies. Finally, section 6 summarizes our conclusions.

2 RUN-UP AND OVERTOPPING EXPERIMENTS

2.1 The run-up of a wave against a wall

According to linear theory, a sinusoidal wave running against a vertical wall will show a maximum elevation at the wall of twice its original crest elevation. This has been confirmed by experiments and numerical investigations by e.g. Smida et al (2011) and Chambarel et al. (2009). In these conditions, there is no run-up jet present. When waves become steeper nonlinear effects will play a

role. The pressure at the wall may then induce accelerations that cause vertical velocities of small amounts of water that are greater than the upward velocity of the water front at the wall, thereby allowing the formation of a jet, as described by Chambarel et al. (2009). The run-up of a wave against a wall was investigated by experiments carried out in MARIN's Concepts basin and has been extensively described by Eikelboom (2016).

Experiments at MARIN

A 2.0 by 2.5 m wall, extending over 50 % of the width and depth of the basin was mounted about 35 m from the wave generator as is shown in Figure 3a. The wave generator was programmed to generate a wave sequence that resulted in a wave group containing a few high waves, preceded and followed by quite small waves, as shown in Figure 3b. Waves with crest elevations up to 0.6 m could be made, and with periods between 1.6 and 2.3 seconds. Note: Measurement of the undisturbed wave took place after removal of the wall, using exactly the same wave generator steering signal, and measuring at the location where the wall had been.

Figure 3: a) View of test set-up from the wave generator: A wall, mounted on a steel frame, extends 0.6 m above water; b) A wave group as used with the running-up wave marked.

The purpose of the tests was to measure the run-up profile and to measure the magnitude of the drops and blobs formed in the spray jet above the wall. A laser scanner was used to measure the water profile at the centerline, while above water, a high-speed video recorded the spray jet. In his thesis, Eikelboom (2016) describes the test setup and compares the measurements with the results of theories for jet break-up and drop size statistics. One of his conclusions was that the run-up spray break-up process is quite different from spray nozzle break-up as is published for example by Ashgriz et al. (2008). The main reason is that the jet thickness is much greater at the wall run-up than in spray nozzles, while in vertical run-up also gravity plays an important role. On the other hand, the analysis of the amounts of drops and blobs, as well as their sizes, resulting in a cumulative mass distribution showed quite good agreement with the root normal distribution, as proposed by Simmons (1977), which was assumed by Aalbers and Poen as a viable approach.

Figure 4: Typical side view of a jet formed at a backward (-15°) inclined wall after run-up.

Figure 4 shows that jets are quite irregular and consequently their thickness could not be measured accurately. Nevertheless, repeated measurements and observations were sufficient indication to substantiate the view that an improved model for the jet volume is required.

2.2 Use of the measurements

The measured profiles were compared with a wave model fitted to the particulars of the incoming and running-up wave, i.e. to the crest height, the preceding trough depth and the trough-trough period. During run-up, the profile is affected by the following five phenomena:

1. Reflected wave volume at the wall
2. Excess kinetic energy in wave crest due to nonlinearity } Pile-up and
3. Enhanced steepness of the wave front due to nonlinearity } Jet forming
4. Volume loss due to water ejected in the spray jet
5. Volume loss when crest height at the wall exceeds wall height → Overtopping

In the next section, an analytical model for the nonlinear wave run-up profile at a wall and the escaping jet is described.

3 NONLINEAR MODEL OF PILE-UP AT THE WALL

The analytical model of the pile-up and the ejection of a jet at the wall is based on the five phenomena listed above, using a numerical 2nd order Stokes wave model combined with the Faltinsen (2002) wedge immersion theory. From Faltinsen's theory basic jet parameters, such as initial speed and root thickness are derived. The present approach models the jet in 'a fluid element time-step' approach including the effects of gravity and overtopping. By comparing the jet volumes calculated from the model with the results of Faltinsen's wedge theory a jet volume correction factor is derived. This correction factor makes the approach suitable for the large statistical sum needed for icing calculations in different sea states, allowing for a large range of wave elevations, periods, directions and drop size distribution classes.

3.1 Wave model

In linear theory, reflection from a wall implies that the incoming wave fully reflects. At the wall an elevation is reached of twice the incoming wave amplitude, and in that instant the kinetic energy is transferred into potential energy at the wall, which in turn transfers into kinetic energy in the opposite direction. The nonlinear wave has a crest which is higher and steeper than a sinusoidal wave, while the troughs are shallower. The 2nd order Stokes wave is the superimposition of a linear wave and a second order bound sinusoidal wave. The wave kinematics in the crest of a linear wave follow the well-known wave equations, but for a nonlinear wave stretching is applied according to the functional stretching method presented by Grue et al (2003). Thus, the exponent e^{kz} is taken into account for z > 0 and the wave particulars are based on the nonlinear trough-trough wavelength λ_{tt} and trough-trough period T_{tt} as driving parameters. These are robust observables in the experiments. The excess kinetic energy ΔE_k, which is present in nonlinear waves due to the applied stretching theory, causes the wave crest to reach higher than twice its original height. The wave crest will, as measured and observed, become more 'triangular' or 'pointed' at the wall and, as observed by Chambarel et al (2009), if sufficient excess kinetic energy is present, a jet will escape.

Defining A_{lin} as the amplitude of the linear wave component, and f as the ratio between crest height and trough depth, i.e. $f = H_c/H_t$, the amplitude of the 2nd order component is obtained by the fraction $(f\text{-}1)/(f\text{+}1)$ A_{lin}. The surface elevation during wave reflection then follows from doubling the cosine wave function with wavelength λ_{tt} , wavenumber $k_x = 2\pi/\lambda_{tt}$ and phase $\varepsilon(t) = 2\pi t/T_{tt}$ as:

$$Z_{wr} = A_{lin}\left(\cos\left(k_x X_{wr} + \varepsilon\right) + \frac{f-1}{f+1}\cos\left(2k_x X_{wr} + 2\varepsilon\right) + k_o\left\{\cos\left(k_x X_{wr} - \varepsilon\right) + \frac{f-1}{f+1}\cos\left(2k_x X_{wr} - 2\varepsilon\right)\right\}\right) \quad (1)$$

Here, k_o is the overtopping ratio that is introduced to account for overtopping, where the wall under an angle θ has a height $h_{wall}\cos\theta$ above water. The overtopping ratio is defined as:

$$k_o = \frac{h_{wall}\cos\theta}{A_{lin}}\left(2 + \frac{f-1}{f+1}\right)^{-1} = \frac{h_{wall}\cos\theta}{A_{lin}}\frac{f+1}{3f+1} \quad (2)$$

Effect of the excess kinetic energy of the 2nd order wave component

Many of the waves in a developing sea state are so steep that they are close to breaking, which occurs when the orbital velocity exceeds the wave celerity $c = \omega/k$. The waves in the run-up tests, with trough-trough wavenumber $k = 2\pi/\lambda_{tt}$, were nearly as steep. To determine the corresponding orbital velocities in the top of the crest, functional stretching is applied using the velocity function

analog to Rozema (2009) for a 2nd order Stokes wave:

$$u_{nl}(x,z,t) = A_{lin} k c_o \frac{\cosh(k(d+z))}{\sinh(kd)} \cos(kx-\omega t) + A_{lin}^2 k^2 c_o \frac{f-1}{f+1} \frac{\cosh(2k(d+z))}{\sinh^4(kd)} \cos(2(kx-\omega t)) \quad (3)$$

In deep water, i.e. for $d > \lambda_{tt}$, the orbital velocity may be simplified using $e^{-2kd} << 1$ as:

$$u_{nl}(x,z,t) \cong A_{lin} k c_o e^{kz} \cos(kx-\omega t) + A_{lin}^2 k^2 c_o \frac{f-1}{f+1} e^{2k(z-d)} \cos(2(kx-\omega t)) \approx A_{lin} k c_o e^{kz} \cos(kx-\omega t) \quad (4)$$

In nearly breaking waves, Grue et al. (2003) apply the following expansions of the dispersion relation and wave celerity to account for the wave crest height $H_c = A_{lin}(1+{}^{(f-1)}/_{(f+1)})$:

$$\omega^2 = gk(1+k^2 H_c^2) \qquad \text{and} \qquad c_{nl}^2 = \frac{g}{k}(1+k^2 H_c^2) \quad (5)$$

Assuming a wave steepness $kH_c < 1$ and applying the Taylor expansion for the resulting root, the difference between the linear and nonlinear wave celerity can be straightforwardly derived as c_{nl}-$c_o \approx c_o \cdot \frac{1}{2} k^2 H_c^2$. On the basis of equation (4), we therefore assume that the orbital velocity in the nonlinear wave crest is changed proportionally and thus:

$$\Delta u(x,z,t) = u_{nl} - u_{lin} = u_{lin} \cdot \tfrac{1}{2} k^2 H_c^2 \quad (6)$$

The crest enhancement during reflection of a nonlinear wave then follows from the energy balance; as the wave impacts the wall, its kinetic energy E_k is transferred to potential energy of water mass in the wave crest. The enhancement of the centre of gravity of the wave crest Δh and the excess kinetic energy ΔE_k are related as $mg\Delta h = \Delta E_k$. In the 2D calculation model, the total excess kinetic energy per unit width can be obtained as the integration of the excess kinetic energy in the fluid elements dS=$dx \cdot dz$ over the crest area S above the linear wave crest at $\frac{1}{2}H_c$:

$$\Delta E_k = \int_S \tfrac{1}{2} m (u_{lin} + \Delta u)^2 - \tfrac{1}{2} m u_{lin}^2 dS, \qquad \text{where} \quad m = \rho dS \quad (7)$$

Consequently, the enhancement of the centre of gravity of the wave crest is obtained as:

$$\Delta h = \frac{k^2 H_c^2}{2g}(1+\tfrac{1}{4}k^2 H_c^2) \int_S u_{lin}^2 dS \quad (8)$$

To obtain a value for the actual crest elevation, it is assumed that the nonlinear wave crest, from which a jet may be ejected as it reaches the wall, has a triangular rather than a sinusoidal shape. The fit of several measured crest roots at the wall shown in Figure 5 supports this assumption. A wave crest enhancement factor f_1 is introduced for the wave approaching the wall. The factor f_2 is the result of the incoming and reflected wave (minus overshoot):

$$H_{c,wall}\big|_{t=0} = f_2 Z_{wr}\big|_{t=0} = \{f_1 + k_o(f_1 - 1)\} Z_{wr}\big|_{t=0} \quad (9)$$

Assuming such triangular shape allows to compute the factor f_1 from the difference Δh in the center of gravity between a linear and nonlinear wave crest, so that:

$$f_1 = \tfrac{3}{8}\pi + \frac{3}{gH_c} k^2 H_c^2 (1+\tfrac{1}{4}k^2 H_c^2) \int_S u_{lin}^2 dS \quad (10)$$

3.2 Jet generation

As the nonlinear wave collides with the wall a jet may be generated. According to the wedge immersion model of Faltinsen (2002) the jet has a root thickness δ_{root} which depends on the geometric angle β between wall and wave surface, known as the dead rise angle in wedge theory, and the linear surface elevation velocity v_{rel} along the wedge side since entry. Whereas the spray jet in Faltinsen's zero gravity model is a narrow tapered shape with a small top angle, the actual jet is slowed down by gravity and thus becomes broader at the top.

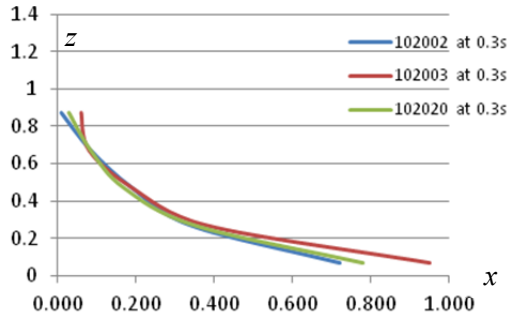

Figure 5: Fit of measured crest and jet-roots at the 0.6 m high wall for 3 repeat waves.

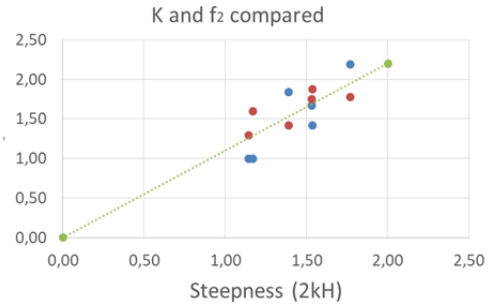

Figure 6: Measured values for K (blue) and f_2 (red)

Aalbers and Poen (2015) simplified the results of Faltinsen's model to an analytical fit. Furthermore, for the application of steep nonlinear waves instead of a falling wedge, they used the wave steepness enhancement factor K introduced by Barlthrop (2005). The root thickness formula they used is:

$$\delta_{root} \cong \tan\beta\left(0.223 - 0.2\beta + \tfrac{1}{15}\left(b - \tfrac{1}{2}\right)^2\right) K \int_{t_1}^{t_2} v_{rel}(t)\,dt \tag{11}$$

The enhancement factor K is easier to handle in the statistical approach of the spray computation of Aalbers and Poen, but otherwise it is similar to f_2 as shown in Figure 6, where both are plotted against wave steepness. If the initial jet velocity is high enough, the jet will escape, but if its initial velocity is relatively low, the initial jet may be overtaken by the wave run-up itself or by faster jet water generated at a later stage of the wave run-up. The present numerical approach uses δ_{root} as input and models the jet as the sum of the contributions from a number of jet volume elements ejected since T_e, as shown in Figure 7.

Method to model a jet under influence of gravity at a given time T

The fluid elements in the jet will follow a ballistic trajectory. A volume element at a given elevation $Z(T)$ and position $X(T)$ is the sum of all elements that have reached that position or have overlap at that position. Consider for example the fluid elements 1 and 2 in Figure 7. Any two-dimensional volume element is assumed to have dimensions $\Delta Z(T)$ and $\Delta X(T)$, which are local sum values of $\Delta Z_i(T)$ and $\Delta X_i(T)$ for one or more jet elements i. The total jet volume at time $T=T_e+idt$ consist of all elements above the crest elevation that are ejected between T_e and T:

$$V_{jet}(T) \cong \sum_i \Delta X_i(T)\,\Delta Z_i(T) \tag{12}$$

The elevation of a fluid element at time $T_e+(i+n)dt$, i.e. for a jet element i ejected at a time idt after T_e and in flight for time ndt, is computed using simple kinematics taking into account a wall inclination θ with respect to the vertical as:

$$Z_i(T) = H_{c,wall}\Big|_{t=T_e} + v_{jet,i}\Big|_{t=T_e+idt} ndt\cos\theta - \tfrac{1}{2} g n^2 dt^2 \tag{13}$$

Or as $Z_i(T) = H_{c,wall}\Big|_{t=T_e+(i+n)dt}$ if the jet element is overtaken by the wave crest equation.

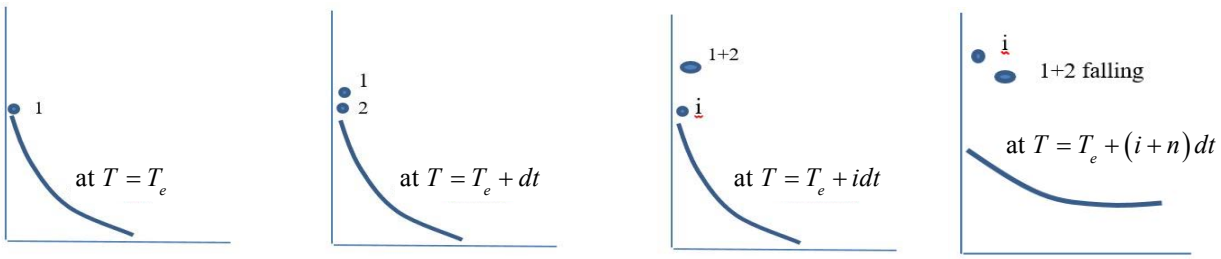

Figure 7: The escaping jet elements may overtake earlier ejected elements.

Water volume in the jet

The local thickness of the jet is computed by using conservation of mass, so that fluid elements spread out horizontally when their vertical velocity reduces. Having a root thickness $\delta_{root,i}$ at time T_e+idt, the thickness and width of the fluid element are thus given by:

$$\Delta Z_i(T) = v_{jet,i}\Big|_{t=T_e+idt} dt\cos\theta - gndt^2 \tag{14}$$

$$\Delta X_i(T) = \delta_{root,i}\left(1-\frac{H_i(T)}{H_{\max,i}}\right)^{-\frac{1}{2}}, \qquad \text{where} \quad H_{\max,i} = \frac{1}{2g}\left(v_{jet,i}\Big|_{t=T_e+idt}\cos\theta\right)^2 \tag{15}$$

Note here that a rectangular shape of the jet elements is assumed. In the summation that yields the local jet element at elevation z and time T, the overlap between elements i and i-1 at elevation z is included. This can be done iteratively also including the element i-2, but for this work one iteration was considered sufficient. The overlap volume is assumed to create additional thickness of the jet. If not overtaken by the wave crest, the volume elements together constitute the volume in the jet, denoted as $V_{jet}(T)$.

Due to water ejected from the wave crest into the jet, the crest elevation reduces. In a practical engineering approximation following Faltinsen's jet model for a wedge, the crest height at the wall reduces by the jet's initial root thickness value $\delta_{root,\ i=0}$. The reduction away from the wall is assumed to be given by the first quadrant of a cosine function with wavelength of $0.5\lambda_{tt}$ and amplitude $V_{jet}(T)$ so as to have conservation of mass. Figure 8 shows computational results of the model in comparison to measurements for a vertical (Figures 8a and 8b) and a forward inclined wall (Figure 8c). It may be concluded that the comparison is quite satisfactory.

3.3 'Drops and blobs' in jet and overtopping

The spray jet is due to a velocity increase of the water along the wall and thus emerges parallel to the wall. When the wave crest exceeds the top of the wall, there will be another jet known as the overtopping jet. In the overtopping jet, the horizontal and vertical velocities of the crest segment that exceeds the top of the wall will be conserved. For small overtopping volumes, the overtopping jet will have low horizontal velocity and will be mixing with the spray jet ejected from below, so that a small amount of water spills over the wall as shown in Figure 8a and Figure 8b. For larger overtopping volumes, the spray jet is effectively cut off and the overtopping jet dominates. For freeboards or wall heights meant to keep most waves out, it is reasonable to assume that only incidentally the top of the crest spills over. Therefore, the effect of overtopping is not considered in the computations in Section 4.

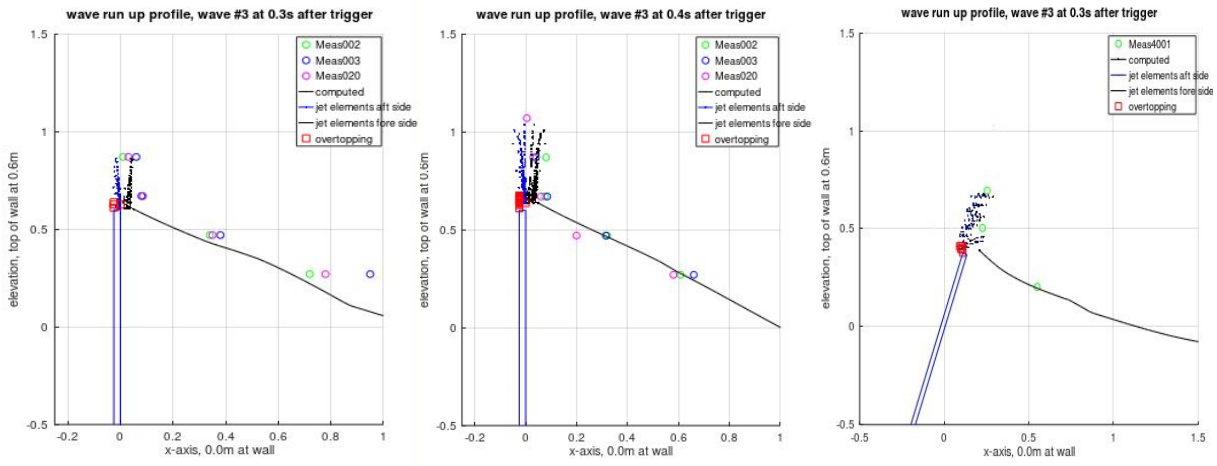

Figure 8: Computed and measured run-up and jet against a: a) vertical wall at 0.3 s after trigger; b) vertical wall at 0.4 s after trigger; c) 20° forward-inclined wall at 0.3 s after trigger.

Jet break-up in 'drops and blobs'

As the spray jet travels upward, a break-up process is started in the jet. Figure 4 and Figure 9 both show the irregular structure of the jet, consisting of local thickness variations and violent break-up in drops and blobs. Eikelboom (2016) has described how the size of the drops and blobs in the jets of the experimental program at MARIN were measured. Figure 10a shows a snapshot of the detection algorithm, which tracks drops in a high speed video and puts markers to them. As time progresses, more and more drops are detected. The break-up of spray jets is presently subject to further research, by means of a PhD study at TU Delft.

Figure 9: Run-up jet from a sloshing experiment breaking up (Bogaert, 2010) showing streaks formed.

According to Simmons (1977) and Ashgriz et al (2008), the cumulative drop volume distribution is best described with a root normal distribution function of drop diameter d versus the 50% of volume drop diameter d_{50} given in Figure 10b. The MARIN experiments also show that this is a valid assumption.

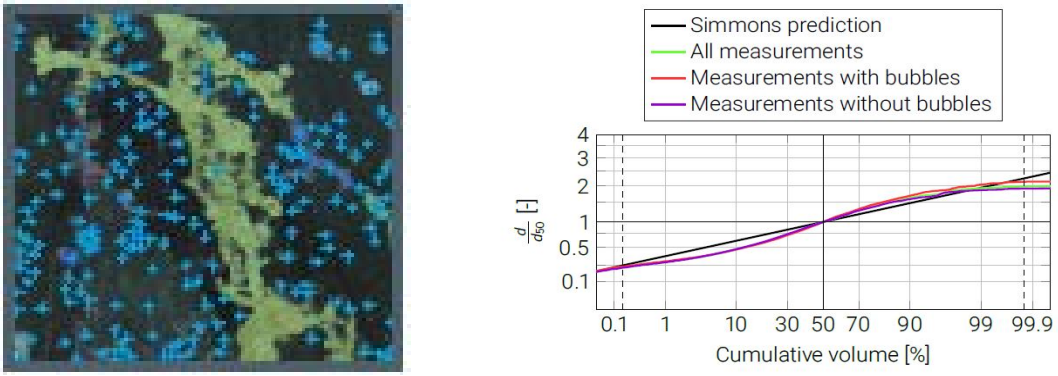

Figure 10: a) Snapshot from high-speed video for drop detection; b) Cumulative drop- volume distribution as a root normal distribution of drop-size ratio

4 APPLICATION TO ICING COMPUTATIONS

Aalbers and Poen (2015) determined the spray volume on basis of the jet root thickness according to the wedge impact theory of Faltinsen (2002). The corresponding jet elevation was obtained by taking into account gravity. The present work shows that the spray jet under gravity tends to assume a plump shape, spreading out at the top. Hereunder, it will be shown that the jet thickness also has a direct influence on the mean drop diameter which is important for the ballistics and deck wetting, and thus for icing.

Difference in jet volume between Faltinsen model and present model

The jet volume is assumed to consist of drops and blobs according to the cumulative root normal distribution considered valid for spray jets. To determine the deck wetting and icing thermodynamics, the trajectory of these water drops and blobs is required in a ship-fixed coordinate system. Accounting for the wind, the water element ballistics determine whether the spray lands in- or outside the ship contours, but also where the spray lands on deck and against which deck structures.

Ashgriz et al (2008) have investigated the droplet size from jet break-up into spray, with the jet caused by fluid flow from a nozzle on a flat plate. They refer to work by Adams (1997) for the mass median diameter d_{mm}, which is the droplet diameter where half of the fluid mass is in smaller drops and half is in larger drops. Aalbers and Poen (2015) have suggested that in order to match with experiments on larger jets the d_{mm} value from Adam's formula should be further enhanced, by a factor $k_2 \approx 2$.

This yields the mass median diameter as:

$$d_{mm} = \left(\frac{3\pi}{\sqrt{2}}\right)^{0.33} k_2 \mu_w^{0.1} v_{jet}^{-0.55} d_h^{0.65} \rho^{-0.21} \sigma_w^{0.24} \tag{16}$$

Here, μ_w is the liquid dynamic viscosity in Pa·s, v_{jet} is the jet velocity, d_h is the nozzle diameter, ρ is the liquid density and σ_w is the surface tension in N/m. The nozzle diameter is considered equivalent to the jet root diameter in Faltinsen's model, δ_{root}. Table 1 below gives the results for a number of typical waves using equation (12) to determine the jet volume.

Table 1: Comparison of volume computation methods

Wave particulars			Velocity	Correction factor C_F	Volume model	
#	H (m)	T_{tt} (s)	$\omega_{tt} H_{t\text{-}c}$		Faltinsen	Present
3	0.46	1.65	1.75	2.50	0.012	0.045
7	0.92	2.23	2.59	1.63	0.038	0.087
4	0.56	1.95	1.80	1.55	0.036	0.089
5	0.44	2.24	1.23	1.21	0.054	0.105
8	0.73	1.85	2.48	1.76	0.019	0.040
9	0.55	1.70	2.03	2.12	0.013	0.035

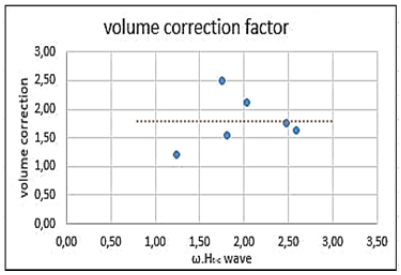

Figure 11: volumes compared with a fit of constant value.

Table 1 shows that a correction factor C_F must be applied on the root thickness δ_{root} from Faltinsen's model. It can be compared with the factor k_2 applied in equation (16), to determine the mass median diameter. A constant value for the correction factor is considered appropriate because the variation of the values show no relation with any of the wave particulars. Henceforth, choosing $C_F = 1.8$, the corresponding k_2 value would be:

$$k_2 = C_F^{0.65} = 1.46 \tag{17}$$

More elaborate correction or taking into account the complete numerical jet model in the icing calculations is a matter of further development, in which also the improved modelling of the break-up process becomes relevant. As these developments are still under investigation, the present work is just indicative of the effect of improved modelling of the jet particulars, i.e. volume and drop size.

5 DISCUSSION

Hoes et al (2016) compared the observed ice accretion on the KV Nordkapp with the results from their 'Shipice' code. The KV Nordkapp sailed in cold weather, east of Svalbard, on a Northern course experiencing heavy icing, as shown by Table 2. The computations in 2016 showed quite acceptable agreement with the observed and measured ice quantities. Presently, the computations are repeated to investigate the effect of the smaller correction factor on drop size and larger jet volume by using the jet volume correction factor C_F and the drop size correction factor given by equation (17). For the icing computation in Shipice, the wetting is assumed to be uniformly spread out over planar elements on deck and vertical walls and the wetting is applied intermittently as averaged wetting per event. For the results presented here, the Shipice code was modified with respect to the dimensions of the superstructure of the ship: Hoes et al used a 10 m high deckhouse over the full width of the ship at 19.7 m behind the bow, which collected large amounts of spray water, while here a 3.2 m high gun platform with a width of 8.4 m was modelled. The dimension and the computed wetting in the period 6-9 hours is shown in Figure 12.

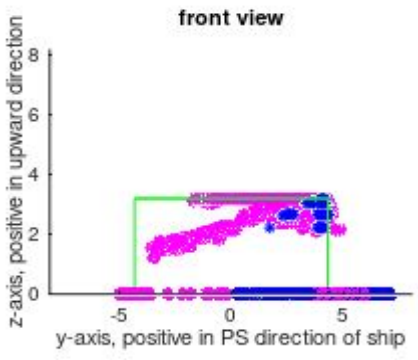

Figure 12: Front side of gun platform and computed wetting.

Table 2: KV Nordkapp data for different time intervals, after Hoes et al (2016).

Parameters	6-9 hr	9-12 hr	12-15 hr	15-17 hr	17-18 hr
Observed icing [mm/h]	23	0	0	17	17
Ship velocity [m/s]	5.2	5.2	4.2	6.2	6.2
Wind velocity [m/s]	16	16	17	15	25
Direction [°degree]	200	210	210	200	200
Significant wave height [m]	7.5-6	5.5	5.5	5.5	5
Air Temperature [°C]	-12.55	-13.3	-15.3	-17.35	-17.35
Relative Humidity [%]	0.84	0.88	0.87	0.87	0.87
Salinity [ppt]	35	35	35	35	35
Sea Temperature (Modeled)[°C]	4.0	3.4	2.75	2.35	2.35

In the intermittent icing process presented by Hoes et al, the effect of run-off was included. On a vertical plane this run-off is quite fast. On a deck, it is governed by camber and ship motions. Furthermore, average roll amplitudes of 4 degrees were assumed. Whereas Hoes et al assumed 10 degrees of deck camber, which is relatively much for a modern vessel, we have obtained additional results for 3 degrees of deck camber. In Table 3, the resulting ice accretion at the front side of the gun platform on the KV Nordkapp is given.

Table 3: Spray onto the front of the gun platform for starboard (SB) and portside (PS). Ice accretion on observation area of gun platform (GP), calculated with Shipice2 for five different time intervals.

	Parameters	6-9 hr	9-12 hr	12-15 hr	15-17 hr	17-18 hr
SB	Spray flux [kg/m2s]	0.001	0.001	0.006	0.0004	0.0004
	Droplet Temperature [◦C]	-6.0	-7.5	-2.3	-15.4	-6.8
PS	Spray flux [kg/m2s]	0.012	0.003	0.033	0.0004	0.007
	Droplet Temperature [◦C]	0.0	2.3	2.1	-9.7	1.6
GP	Ice rate (Shipice2 – 10 dgr) [mm/hr]	0.2	2.8	17.1	1.0	10.4
	Ice rate (Shipice2 – 3 dgr) [mm/hr]	3.0	7.4	23.7	1.2	11.1

Any water landing on the top of the gun platform will run off at the front and sides. This causes a 'second wetting' some time after the initial spray event. It is difficult to include this in the current model, but could be worthwhile investigating. Based on a crude engineering estimate, it is assumed that run-off from the gun deck towards its front side is about 15%, and that it causes icing at the same 'wetting volume to ice volume ratio' as the initial spray events. In the results given by Table 3 and Figure 13 this estimate is included.

In addition to the newly obtained results, referred to as Shipice 2, Figure 13a also includes former results from Hoes et al (2016), referred to as Shipice 1, and Samuelsen et al. (2015), denoted as ModStall and the 'test model'. The main difference between Shipice and the other models is that it uses a sea-keeping model to quantify the amount of spray, while the models discussed in Samuelsen et al used an estimated spray flux of 0.055 kg/m^{2}s and a single size of 2 mm for all droplets. As a consequence, in these models, all droplets arrive at the ship with the same temperature of -2.5 ºC.

Spray flux, diameter and corresponding temperature of the droplets are of great importance for the icing accretion, as shown in Table 3. In the Shipice2 calculations, the temperature of the droplets arriving at the deck house front vary strongly between +2.3 and -15.4 ºC. It appears that the lowest temperatures coincide with small amounts of spray, which are caused by thinner spray jets and thus smaller droplets that cool stronger in the cold air, and that a longer traveling distance to starboard gives more cooling.

The final icing amount following from the Shipice2 computations compare quite well with the observed icing thickness at the front of the gun platform, but the accretion over time is different. The main cause for this difference is the local amount of wetting: between 12h00 and 15h00, the spray flux on the front deckhouse is about a factor 10 larger than at other times, while this is not apparent from the observed icing growth. Another factor that has contributed to differences in the

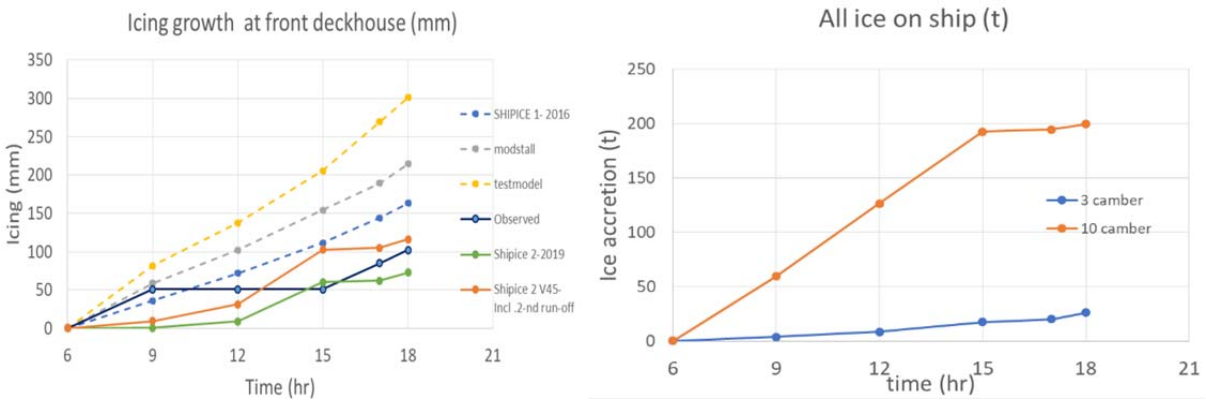

Figure 13: a) Observed and computed icing growth on the deckhouse front; b) Icing accretion on the whole ship, effect of 3° and 10° deck camber, both with 4° roll.

observed and calculated ice accretion rate at the deckhouse front are changes in heading and ship speed and between 12h00 and 15h00. Additionally, due to wind speeds increasing up to 25 m/s during the last hour while the wave height reduced, the spray flux increased and spray water landed at different locations on deck. The influence of this can also been seen in Figure 13b that shows a fairly constant overall icing rate between 6h00 and 15h00.

Another important aspect is the water run-off from the deck surfaces. The computations indicate that the fore deck of the KV Nordkapp must have experienced intensive flooding due to the large blobs of water in the lower part of the run-up spray jet. The rate at which this water runs off the deck and over the side depends on ship motions and deck camber; at high run-off rates, much time is left for a remaining water film to freeze onto the deck, while at low run-off rates, the relatively warm sea water will change the thermodynamic balance on deck. This causes the existing ice layer to slightly melt first, which then requires time to re-freeze, so that the time left for additional icing to occur before the next spray event is reduced. The resulting icing accretion on deck is therefore much less with a 3° deck camber than with a 10° deck camber as shown by Figure 13b. Here, for both cases a 4° roll amplitude was used. This result shows that it may be useful to keep water on deck longer to reduce the deck icing, for example by partly closing some of the freeing ports.

6 CONCLUSIONS

The analysis of experiments of wave run-up against a wall has resulted in a practical engineering model for water pile-up against the wall and jets escaping the wave run-up leading to spray of significant water volumes. The pile-up and jet model successfully apply the principles of 2nd order Stokes wave theory and gravity. The model is suitable for stochastic predictions of spray in an irregular seaway. Run-off paths of spray water, e.g. over the side of the deck house are not included in the model but could be a valuable extension of the method.

By applying a simple correction factor to the jet volume above the ship freeboard, the results have been made applicable to icing computations as were earlier presented by Hoes et al (2016). The results for the icing growth computations with the updated model are compared to the icing growth observed at the KV Nordkapp. The results show that the updated model, at least in average sense, performs better than the former model and additionally is better able to predict the icing accretion than some of the other models currently available in literature.

REFERENCES

Aalbers, A.B. & Poen, G.J., 2015. Probabilistic Modelling of Marine Icing: an Estimation Method for Spray Water. *Proceedings OTC 22536*.

Ashgriz, N., Ahmed, M., & Tran, H., 2008. Characterization of black liquor sprays from splash plate nozzles. *Engineering Pulping & Environmental Conference*, TAPPI.

Adams, T.N., 1997. Kraft Recovery Boilers, chapter 4, pages 103–127. TAPPI Press.

Barlthrop, N. , 2005. HSE-UK: Wave slap loading on FPSO bows. *Research report 324*, University of Glasgow and Strathclyde.

Bogaert, H., Léonard, S., Brosset, L., & Kaminski, M.L., 2010. Sloshing and scaling: results from the Sloshel project. *Proceedings ISOPE 20*, Beijing, China.

Buchner, B., 1998. A New Method for the Prediction of Nonlinear Relative Wave Motions', *Proceedings OMAE*, Lisbon.

Buchner, B. & Voogt, A., 2004. Wave Impacts due to Steep Fronted Waves. *Rogue Waves Symposium*, Brest, France.

Buchner, B., Bunnik, T.H.J., Fekken, G. & Veldman, A.E.P., 2001. A Numerical Study on Wave Run- up on an FPSO Bow. *Proceedings OMAE*, Rio de Janeiro.

Chambarel, J., Karif, C. & Touboul, J., 2009. Head on collision of two solitary waves and residual falling jet formation. *Nonlinear Processes in Geoph.*, European Geosciences Union.

Eikelboom H., 2016. Verification and validation of a spray water model for maritime structures'. *MSc thesis*, TU Delft.

Faltinsen, O., 2002. Water entry of a wedge with finite dead rise angle. *Journal of Ship Research*. Vol. 46, No. 1.

Fekken, G., 2004. Numerical simulation of free-surface flow with moving rigid bodies. *PhD Thesis*. RU Groningen.

Grue, J., Clamond, D., Huseby, M. & Jensen, A., 2003. Kinematics of extreme waves in deep water. *Applied Ocean Research* 25.

Hoes, C.M., Aalbers, A.B. & Hoving, J.S., 2016. Modelling the ballistics and thermodynamics of bow spray droplets for marine icing, *Proceedings OTC* 27405.

Horjen, I., 2015. Offshore drilling rig ice accretion modeling including a surficial brine film. *Cold Regions Science and Technology* 119.

Hofland, B., Diamantidou, E., van Steeg, P. & Meys, P., 2015. Wave run-up and wave overtopping measurements using a laser scanner. *Coastal Engineering* 106.

Kulyakhtin, A., 2014. Numerical Modelling and Experiments on Sea Spray Icing. *PhD Thesis* NTNU, Trondheim,

Noblesse, F., Delhommeau, G., Yeng, C., Kim, H.Y. & Queuley, P., 2011. Analytical bow waves for fine ship bow a with rake and flare. *Journal of Ship Research*.

Ogawa, Y., Taguchi, H. and Ishida, S., 1998. A Prediction Method for the Shipping Water Height and its Load on Deck. *PRADS'98*, The Hague.

Rozema, W., 2009. *BSc Thesis* Groningen University.

Samuelsen, M., Løset, S. and Edvardsen, K., 2015. Marine icing observed on KV Nordkapp during a cold air outbreak with a developing polar low in the Barents sea. *Proceedings International Conference on Port and Ocean Engineering under Arctic Conditions* 23, 2015.

Simmons, H.C., 1977. The correlation of drop-size distributions in fuel nozzle sprays - part i: The drop-size/volume-fraction distribution. *Journal of Engineering for Power*, 99(3):309.

Smida, K., Lamloumi, H., Hafsia, Z. & Maalel, K., 2011. CFD analysis of water solitary wave reflection. *Journal of Engineering Research* Vol. 8, No. 2.